Nonlinear dynamics of a semiconductor laser with filtered optical feedback and the influence of noise

Mirvais Yousefi* and Daan Lenstra
Vrije Universiteit, FEW N&S, De Boelelaan 1081, 1081 HV Amsterdam, The Netherlands

Gautam Vemuri
Department of Physics, Indiana University, Purdue University, Indianapolis (IUPUI), Indiana 46202-3273
(Received 25 November 2002; published 23 April 2003)

We investigate the influence of quantum noise on the highly complex nonlinear dynamics that arise in a single-mode semiconductor laser subject to filtered optical feedback. Our numerical study, which utilizes rate equations that are augmented by Langevin noise terms to account for the spontaneous-recombination noise, shows that for relatively broad filters the noise may lead to qualitatively different dynamics than predicted by a deterministic analysis. In particular, we find that certain attractors that are predicted in the absence of noise may no longer be available when the effects of noise are correctly incorporated. For narrow bandwidth filters we demonstrate optical-injection-like behavior and identify locking of the semiconductor laser to the relaxation oscillation side peaks. In general, the results indicate that shot noise in the laser can influence the dynamics quite substantially.

DOI: 10.1103/PhysRevE.67.046213 PACS number(s): 05.45.−a, 42.55.Px, 42.65.Sf, 42.65.Pc

I. INTRODUCTION

Optical feedback induced dynamics in semiconductor lasers have attracted considerable attention in recent years [1–15]. It is now a well-known fact that such lasers exhibit rich nonlinear dynamical behavior [1,2], involving steady-state cw operation (fixed-point dynamics), self-oscillations (limit cycle dynamics) [3], quasiperiodicity [4], and chaos [5]. Various types of coexistence have also been predicted with complicated bifurcation schemes [6]. Several early studies dealt with conventional optical feedback (COF) [3,6–8], where the spectral content of the light that is fed back into the laser is not altered. COF, under the right conditions, is routinely used to improve the frequency stability of a semiconductor laser by coupling the laser to a high-finesse resonator [9,10]. More recently, motivated by a number of factors, filtered optical feedback (FOF) has become a topic of interest [11–14]. Among the obvious reasons for pursuing an analysis of FOF is the fact that in many applications a semiconductor laser is subject to optical feedback from a diffraction grating, or from a resonant medium such as a vapor cell, which spectrally filters the feedback light. From the nonlinear dynamical perspective, which constitutes our interest in this subject, spectral filtering of the feedback light has some profound implications on the response of the laser. The complex dynamical behavior in lasers with feedback is primarily rooted in the undamping of the intrinsic relaxation oscillation in the laser in combination with the relatively large phase-modulation property of semiconductor lasers (expressed by the α parameter). A filter with an appropriately chosen bandwidth can provide a mechanism for controlling the influence of relaxation oscillations on the dynamical response. Furthermore, the use of a filter to control the frequency content of the feedback light introduces a controllable nonlinearity into the feedback system, where the nonlinearity is due to the response function of the filter. The ability to exploit this nonlinearity, and hence control the dynamics of the laser, arises from the fact that one now has two parameters that can be varied, the filter bandwidth and the detuning of the filter from the solitary laser frequency. A judicious choice of these two parameters, which are external to the laser, allows one to choose the point of the operation on the nonlinear response function of the filter and hence affect the dynamics of the laser.

The original interest in optical feedback arose from a desire to understand the associated instabilities, and to develop strategies for controlling the underlying dynamics [6–10,15,16] so as to achieve narrow linewidth operation. Later, it became evident that in certain instances these instabilities can have practical applications as well, such as the application of coherence-collapse dynamics in CD players and pump lasers, and the more recent subject of chaotic encryption in which a low-frequency fluctuations attractor is used to produce the carrier wave [17–20].

We now discuss the motivation behind pursuing an elucidation of the role of noise in influencing the dynamics of a semiconductor laser that is subject to filtered optical feedback. Deterministic analyses of FOF have predicted a rich variety of dynamics and also coexistence of attractors over a large parameter range [11,14]. However, in such an analysis, there is no guarantee that a predicted attractor is stable, or what its relative stability is with respect to another attractor. Since the noise levels in semiconductor lasers are relatively high, both below and above threshold, it is reasonable to speculate that these noise levels will affect the dynamical response of the laser. Intuitively, one expects that noise will drive the laser dynamics to the most stable attractor and so, through a noise analysis, one can obtain some indirect knowledge of the relative stability of coexisting attractors. Close to bifurcations, and in instances with coexisting dy-

*Email address: mirvais@nat.vu.nl

namical attractors, the issue of stability may become so crucial that in order to accurately predict the dynamics one must include the effect of noise. At the very least, therefore, a noise analysis may help identify which of the attractors that are predicted by a deterministic analysis are marginally stable, and which are robust.

An elucidation of the noise effects is also important if one is to implement the nonlinear dynamical behavior of a semiconductor laser in applications like chaos control, chaos synchronization, and chaotic encryption [18–20]. Lastly, noise in nonlinear systems often causes some unexpected and unusual dynamics, and a systematic elucidation of the effect of noise on the response of a semiconductor laser is therefore useful.

In this paper, we will consider noise due to the combined effects of carrier recombination and spontaneous photon emission into the laser mode. The rate of the latter process is usually a small fraction (Petermann factor) of the total carrier-recombination rate. These noise sources are quantum mechanical in origin and are additive. There can also be contributions from multiplicative technical noise that can arise from fluctuations in injection current or laser temperature. However, these are neglected in this paper since these sources of noise can be mitigated. It was shown by Henry [21], and later confirmed by Petermann [16], that in a single-mode semiconductor laser the influence of carrier shot noise on the laser linewidth in *cw operation* can be neglected. Our work indicates that, while the role of shot noise is indeed marginal in determining the steady-state characteristics of the laser, one cannot say the same about its effect on the dynamics. In fact, one of our principal findings is that the carrier shot noise, despite its relatively small magnitude, has a profound effect on the *dynamics* of the laser, and so it is crucial that one include the shot noise contribution when studying the feedback-induced dynamics of a semiconductor laser.

In related work, we previously identified three distinct regimes of interest depending on the relative values of the filter bandwidth, the relaxation oscillation frequency of the laser, and the external cavity mode spacing induced by the external delay. The first, called the narrow filter case, is the regime where the filter bandwidth is much less than the relaxation oscillation frequency, and the external cavity mode spacing, and so the laser is expected to operate on the single external cavity mode that lies within the filter spectral profile. If the magnitude of the filter bandwidth lies between the external cavity mode spacing and the relaxation oscillation frequency, the intermediate bandwidth regime, the complexity of the dynamical behavior is enhanced since many more attractors are now available to the laser. Lastly, if the filter bandwidth is much larger than the relaxation oscillation frequency and the external cavity mode spacing, the broad filter case, the laser response mimics behavior under COF and one would observe even more complicated dynamics.

Of the three cases mentioned above, the intermediate filter case is the one that evinces most interest since the dynamics are substantially different from those due to COF and yet they are significantly more complex than those due to a narrow filter. Using the deterministic dynamics that arise for such filters as a reference, this paper will, in a later section, investigate the noise-induced alterations to the dynamics.

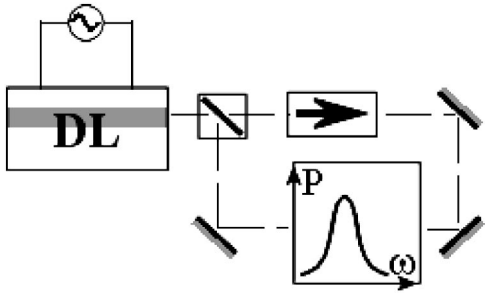

FIG. 1. Sketch of the unidirectional ring configuration for the filtered optical feedback setup under study. The light emitted by the semiconductor diode laser (DL) passes through a beam splitter, an optical isolator, the frequency filter, a second optical isolator, and an attenuater, which can be used to control the amount of feedback. After the attenuater the light is sent back to the semiconductor laser via the beam splitter.

For an elucidation of the noise effects on laser dynamics, we find the narrow filter case to be of interest also. This is especially so because the dynamics are much less complex than for wider filters, and hence allow one to focus on the effects of noise. Furthermore, with narrow bandwidth filters, one expects the frequency content of the noise to be filtered, thereby approximately reproducing the situation that arises during optical injection, i.e., when an external, monochromatic light is injected into the laser. The analogy with optical injection is particularly appealing because there is a vast literature on the deterministic aspects of this topic that can be used as comparative reference to gauge the effects of noise [22]. The value of such comparisons can be emphasized by noting that the feedback system is mathematically very complex, and so one is mostly restricted to a simulation of the dynamics. In such instances, a connection of the feedback system with the injection system can be essential for a thorough elucidation of the noise-induced dynamics in a semiconductor laser.

In the next section we describe the theoretical model that was used in this work to determine the effect of noise on the dynamics of a semiconductor laser under FOF. That is followed by Sec. III, which contains a summary of deterministic dynamics, reviewing the notion of external cavity modes and fixed points. Section IV describes the noise-induced dynamics in the laser, for both intermediate and narrow filter widths, and the final section contains a summary and discussion of the principal points of the paper.

II. MODEL

Figure 1 contains a schematic sketch of a FOF setup which consists of the semiconductor laser, an external delay line, and a frequency-selective filter. The external delay line also includes two optical isolators and an attenuater to emphasize that we assume unidirectional propagation of the light in the delay line and that the amount of feedback is controllable. To mathematically describe this system, we augment the single-longitudinal mode model for a laser with

TABLE I. The parameter values used in the simulations.

Quantity	Symbol	Value
Linewidth enhancement factor	α	5
Feedback rate	γ	13.07×10^{9} or 0.653×10^{9} s^{-1}
External cavity round-trip time	τ	3 or 1.5 ns
Differential gain coefficient	ξ	5×10^{3} s^{-1}
Photon decay rate	Γ_0	10^{11} s^{-1}
Carrier decay rate	T_1	1 ns
Threshold pump rate	J_{thr}	1.4×10^{17} s^{-1}
Pump rate	J	$\sim1.5J_{\mathrm{thr}}$
Average carrier pair number	$\langle N(t)\rangle$	$\sim10^{17}$
Spontaneous emission rate	R	5×10^{12} s^{-1}
Pump-rate-induced frequency shift	k	1.25×10^{-6}

FOF that was used in Ref. [14], with Langevin noise terms $[L_E(t),L_n(t)]$ that model the spontaneous-recombination noise in the laser. As alluded to previously, we assume that any technical noise, such as refractive index fluctuations in the delay line or thermal fluctuations in the filtering element, can be neglected compared to the spontaneous-recombination noise inside the semiconductor laser. The filter is assumed to have a Lorentzian spectral profile, which is a convenient approximation that permits simplifications in the numerical model. In practice, a diffraction grating, or a Michelson or Fabry-Pérot interferometer, would serve as the filter, and in such cases the assumption of Lorentzian filter response ignores the effect of the filter's free spectral range and its multiresonant nature. Nonetheless, we found in previous work that a model with a Lorentzian spectral filter mimics many of the experimentally observed features when a Fabry-Pérot filter is utilized and hence is a very good approximation.

The optical field in the laser is represented by $E(t)=E(t)\exp\{i\omega_0 t\}+\mathrm{c.c.}$, where ω_0 is the operation frequency of the laser in the absence of feedback (to be referred to as the "solitary laser"), while $E(t)$ is the (complex) slowly varying amplitude. The model equations read

$$\dot{E}(t)=\frac{1}{2}(1+i\alpha)\xi n(t)E(t)+\gamma F(t)+L_E(t), \tag{1}$$

$$\dot{F}(t)=\Lambda E(t-\tau)\exp(-i\omega_0\tau)+(i\omega_m-\Lambda)F(t), \tag{2}$$

$$\dot{n}(t)=J-J_{\mathrm{thr}}-\frac{n(t)}{T_1}-[\Gamma_0+\xi n(t)]|E(t)|^2+L_n(t), \tag{3}$$

$$\omega_0=\omega_{\mathrm{thr}}-k(J-J_{\mathrm{thr}}). \tag{4}$$

Here, $F(t)$ is the (complex) field amplitude in the external system after filtering and before reentering into the laser cavity, and $n(t)$ describes the inversion, or the number of electron-hole pairs relative to their value at solitary laser operation. Λ is the half width at half maximum (HWHM) of the (Lorentzian) filter, ω_f is the central frequency of the filter, and ω_m is the relative detuning between the center frequency of the filter and the solitary laser frequency, i.e., $\omega_m\equiv\omega_0-\omega_f$, $J=I/e$ is the normalized pump rate, I is the pump current, e is the unit charge, J_{thr} is the pump rate at the solitary laser threshold of the specific longitudinal mode, ω_{thr} is the corresponding threshold frequency, and k (>0) is an empirical constant of proportionality. In principle, since the gain coefficient ξ depends on frequency, it will show variations with the pump rate as well. However, as we do not expect any significant effect resulting from the modest frequency variation range here considered (20 GHz), the gain coefficient is taken constant. Finally, T_1 denotes the carrier decay time.

Equation (4) accounts for the frequency shift induced by a change in the pump current. Unlike COF the solitary laser frequency cannot be taken as reference since there now exists a second optical frequency in the system, i.e., the filter center frequency (ω_f). The changes in refractive index and temperature, induced by the pump current, will alter the solitary laser frequency. This combined drift is known to decrease with increasing pump current and its magnitude is expressed in Eq. (4) by the positive empirical constant k.

The last terms in the right-hand sides of Eq. (1) and Eq. (3) are the Langevin noise terms, which represent the random fluctuations due to spontaneous recombination noise. Their correlation properties are

$$\langle \mathrm{Re}\,L_E(t)\,\mathrm{Im}\,L_E(t')\rangle=0, \tag{5a}$$

$$\langle \mathrm{Re}\,L_E(t)\,\mathrm{Re}\,L_E(t')\rangle=\langle \mathrm{Im}\,L_E(t)\,\mathrm{Im}\,L_E(t')\rangle=R\,\delta(t-t'), \tag{5b}$$

$$\langle L_n(t)L_n(t')\rangle=D\,\delta(t-t'), \tag{6}$$

where δ is the Dirac delta function, R the rate of spontaneously emitted photons into the semiconductor-laser longitudinal mode under consideration and D the shot noise diffusion strength, which is proportional to the average amount of carriers in the device over one carrier lifetime (T_1). In the simulations the spontaneous-recombination rate was chosen such that the resulting solitary laser linewidth was $\sim$20 MHz at 50% above threshold (see Table I). The Langevin force L_n represents the influence of recombination shot noise on the inversion while L_E represents the effect of spontaneously emitted photons into the lasing mode. The cross correlation

between L_E and L_n is very small since only a small fraction ($\beta \approx 10^{-5}$) of recombination events leads to a photon ending up in the lasing mode [16], and has therefore been neglected.

All other parameters are identified in Table I. Writing $E(t) \equiv \sqrt{P(t)} e^{i\phi(t)}$, where $\phi(t)$ and $P(t)$ are the slowly varying phase and power, the normalization is such that P equals the number of photons inside the laser. Consistent with this normalization, n represents the inverted population (the number of excess electron-hole pairs in the active layer).

III. DETERMINISTIC DYNAMICS

In this section we briefly review our previously reported work on the deterministic dynamics that result in a semiconductor laser due to FOF. In particular, we draw attention to the fact that the filter parameters can be effectively used to control the feedback light and hence alter the complexity of the dynamics. The simplest modes of operation of the FOF laser system are those corresponding to single-frequency (cw) light emission. These are often referred to as external cavity modes (ECMs), and we will follow this nomenclature here. In dynamical-systems language the ECMs are derived from the fixed points of Eqs. (1)–(3) with Langevin terms set to zero, i.e., the solutions of the form

$$E(t) = \sqrt{P_s} \exp[i \Delta\omega_s t], \tag{7}$$

$$F(t) = \sqrt{Q_s} \exp[i(\Delta\omega_s t + \theta_s)], \tag{8}$$

$$n(t) = n_s, \tag{9}$$

where P_s, Q_s, $\Delta\omega_s$, θ_s, and $n_s \in \mathcal{R}$ are time-independent quantities and $P_s, Q_s \geqslant 0$. A closed transcendental equation for the frequency shift $\Delta\omega_s$ from the solitary laser frequency ω_0 can be derived, reading

$$\Delta\omega_s \tau = -C_{\text{eff}} \sin[\Delta\omega_s \tau + \omega_0 \tau + \arctan(\alpha) - \arctan[(\Delta\omega_s - \omega_m)/\Lambda], \tag{10}$$

where

$$C_{\text{eff}} = \frac{\gamma\tau\Lambda\sqrt{(1+\alpha^2)}}{\sqrt{\Lambda^2 + (\Delta\omega_s - \omega_m)^2}}. \tag{11}$$

In Fig. 2, the fixed-point frequencies $\omega_s \equiv \omega_0 + \Delta\omega_s$, are plotted versus the solitary laser frequency ω_0. From Eq. (4) it can be seen that moving from left to right in this figure corresponds to decreasing the pump current. Each intersection of a straight vertical line with the continuous, multivalued, and oscillating curve in Fig. 2 corresponds to a fixed-point solution at that specific pump current (solitary laser frequency). Two such examples are shown in the (η, P) plane in the insets to Fig. 2, where P is the photon number and $\eta \equiv \phi(t) - \phi(t-\tau)$ is the phase difference between the light emanating from the laser and the feedback light. Note that the vertical line labeled ''a'' intersects the oscillating curve at 11 locations, each of which corresponds to one of the fixed points shown in inset (a). The insets also show the solitary laser mode, denoted by a diamond. Similarly, vertical line ''b'' in Fig. 2 intersects the oscillating curve at nine points, thereby leading to nine fixed point in inset (b). Note that vertical line ''a'' is closer to the center of the filter and hence leads to more fixed points than at the location of line ''b.'' It is also clear from inspection of Fig. 2 that a vertical line in the wings of the filter (not shown) will intersect the oscillating curve at very few points, implying that the number of fixed points in the tails of the filter would be small. Since the complexity of the dynamics is directly related to the number of fixed points available, Fig. 2 shows that the filter detuning, and its bandwidth, can be used to control the observed dynamics. Physically, changes in the bandwidth of the filter have a similar effect, since increasing the bandwidth increases the amount of feedback light and leads to more complex dynamics (periodic and quasiperiodic oscillations and chaos). An extensive discussion of the fixed points, their stability, their detuning dependence, and the α-induced asymmetry can be found in previous work [14].

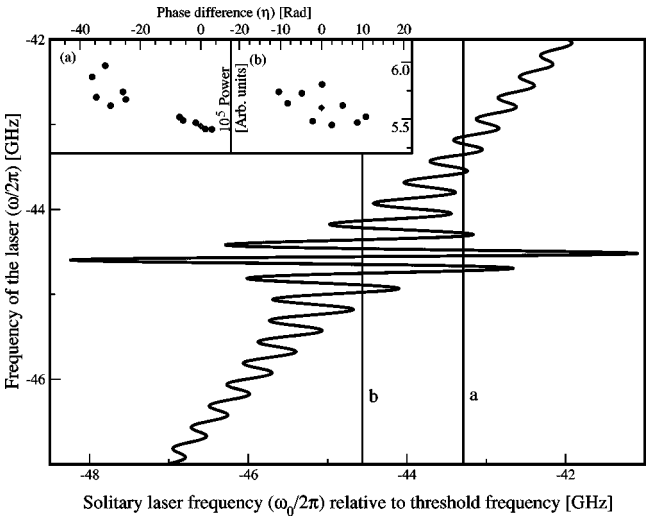

FIG. 2. Fixed-point solutions to Eq. (10) in the (ω_s, ω_0) plane. The insets show the fixed points in the (η, P) plane for the two cases (a) and (b) as indicated in the main frame. In (a) the detuning is large enough to split the fixed-point body into two separate islands, creating a potentially globally bistable situation. In (b) the filter profile is seen to be superimposed on the standard COF fixed-point ellipse.

IV. RESULTS

To investigate the effects of quantum noise on the dynamics of a semiconductor laser that is subject to FOF, we integrated Eqs. (1)–(3) with a modified Runge-Kutta method of second order. The noise was simulated by a standard random generator [23], which returns a uniform Gaussian random deviate with zero mean and unit variance. It uses a subtractive method [24] to calculate uniform deviates in the interval (0.0,1.0) from which the Gaussian deviates are calculated. These deviates were multiplied by the noise diffusion strengths to get the desired amplitude of the noise source. Since the noise is assumed to be Gaussian, defining the first two moments is sufficient for a complete description of the stochastic process because the higher-order moments are re-

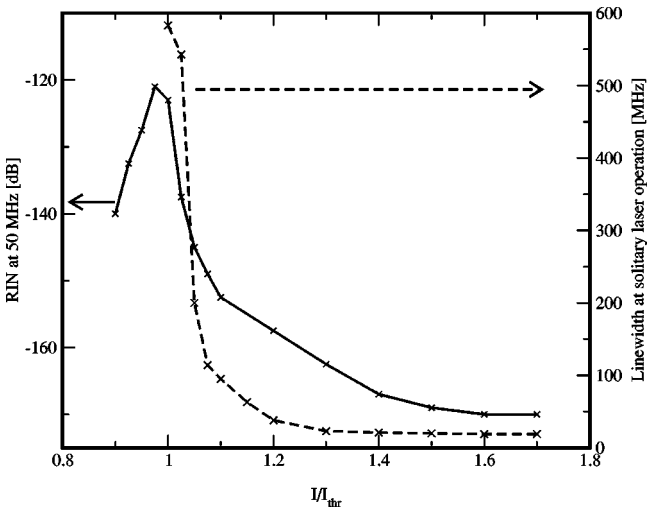

FIG. 3. RIN and linewidth (FWHM) calculations for a solitary laser in the presence of noise as described by Eqs. (1)–(3). The left vertical axis indicates the level of the RIN at 50 MHz in dB, while the right vertical axis indicates the linewidth of the solitary laser in MHz.

lated to the first two. As in Ref. [14], a Poincaré-map-like intersection of the phase space trajectory with a (predefined) plane is recorded together with the average value of the trajectory over 50 external cavity round trips. For each phase space trajectory, we recorded a histogram of the possible η values, and where relevant also calculated the optical spectrum of the laser field.

Figure 3 contains the spectral linewidth of the solitary laser in cw operation (right vertical axis), and the relative intensity noise (RIN) at 50 MHz, as a function of pump current (left vertical axis), which can be used to gauge the effect of our chosen noise parameters on the steady-state characteristics of the laser. For these results, the spontaneous emission rate was set to $R=5\times10^{12}\ \mathrm{s}^{-1}$ and $D=1.45\times10^{16}\ \mathrm{s}^{-1}$, so as to achieve a relatively low-shot-noise laser. Consistent with the well-known and expected behavior (see, e.g., [16] and [21]), the linewidth decreases with increasing pump current [the (artificial) saturation at high pump levels is a consequence of our numerical accuracy]. Indeed, the spectral linewidth remains unaffected as D is increased up to $D\sim10^{18}\ \mathrm{s}^{-1}$ (not shown). Also, the buildup of coherence is clearly observed in the low-frequency RIN, which decreases with higher pump levels.

When several states of operation are simultaneously available to a dynamical system, it is called multistable. It has been shown that the FOF system exhibits multistability [11,12,14], and the final state of operation depends on which basin of attraction of a specific attractor one starts in. In the analysis of delay systems one generally projects an infinite dimensional phase space trajectory onto a finite dimensional phase space, the (η, P,n) phase space in our case. We will analyze the system in this restricted phase space and therefore identify mathematical quantities such as the basin of attraction in the same environment. Due to the $E(t-\tau)$ term in Eq. (2) the system of Eqs. (1)–(3) is infinite dimensional. To integrate these from $t=0$, an integrable function $g(t)$, defined over the interval $-\tau\leqslant t<0$, is required as an initial condition [1]. For the sake of consistency and due to the shadow-ability considerations [25], we require that the initial conditions $g(t)$ are part of a phase space trajectory in both the full and our restricted phase space. This requires $g(t)$ to be differentiable [1], and since it is impossible to ''guess'' a τ-long, differential piece of trajectory in the restricted phase space we use the fixed points as initial conditions. From there, numerical noise will drive the system to shadow a real phase space trajectory [25].

The argument that inclusion of noise in the FOF simulations can effectively serve as a stability analysis of the available attractors can be qualitatively motivated as follows: the phase space can be compared with a potential landscape consisting of (stable) valleys separated by (unstable) hills. In order to operate on a specific attractor, i.e., reside within a valley, the phase space trajectory must be within its basin of attraction. Due to the stochastic nature of the system, a transition from one basin of attraction to another is possible depending on the ratio of noise strength to the ''potential barrier'' to be surpassed. Escape from a valley will occur if the noise amplitude is large enough to overcome the ''hill'' separating one valley from the next. Here, the shot noise strength plays a key role in that most of the multistable attractors derived from deterministic analysis happen to be nonexistent in the presence of noise, since the potential barriers separating the original attractors are small and can be overcome. Therefore, inclusion of noise eliminates the unstable attractors and, for the few attractors that do survive, the final state of operation, i.e., which attractor the system resides in, still depends on initial conditions.

To illustrate the above discussion we chose a situation where the external delay time is 3 ns and the filter bandwidth falls in the intermediate range, i.e., $\Lambda\sim2$ GHz. We begin with the noise-free case and choose parameters that lead to the three coexisting attractors shown in Fig. 4(a), viz., a torus (*a*), a limit cycle (*b*), and a chaotic attractor (*c*). The inset to the figure also shows time series of power for the three attractors in which the fast oscillations are on the relaxation oscillation time scale while the slow oscillations in *a* and *c* are approximately at the external round trip (delay) time scale. Note that the horizontal scale in *c* is different from that in *a* and *b*. Below the phase space portrait, the histogram of η values is given for the three attractors. Each histogram contains the η statistics of the motion of the phase space trajectory on a specific attractor over 10 round trip times. Therefore, the attractors can be compared for the different noise strengths in Figs. 4(a)–4(d), but conclusions on the relative stability of attractors cannot be extracted. The histograms show that during chaotic operation (labeled *c* in the phase space) the system mainly resides at $\eta\approx-30$, but occasionally the trajectory passes very close to the limit cycle [also seen in the projection of Fig. 4(a)]. Note that Fig. 4(a) also displays the fixed points that result from a deterministic analysis.

We next show, in Fig. 4(b), the dynamics of the laser when spontaneous emission noise ($R=5\times10^{12}\ \mathrm{s}^{-1}$) is included in the model. The shot noise is still set equal to zero, i.e., $D=0$. Note that the phase space trajectories look similar

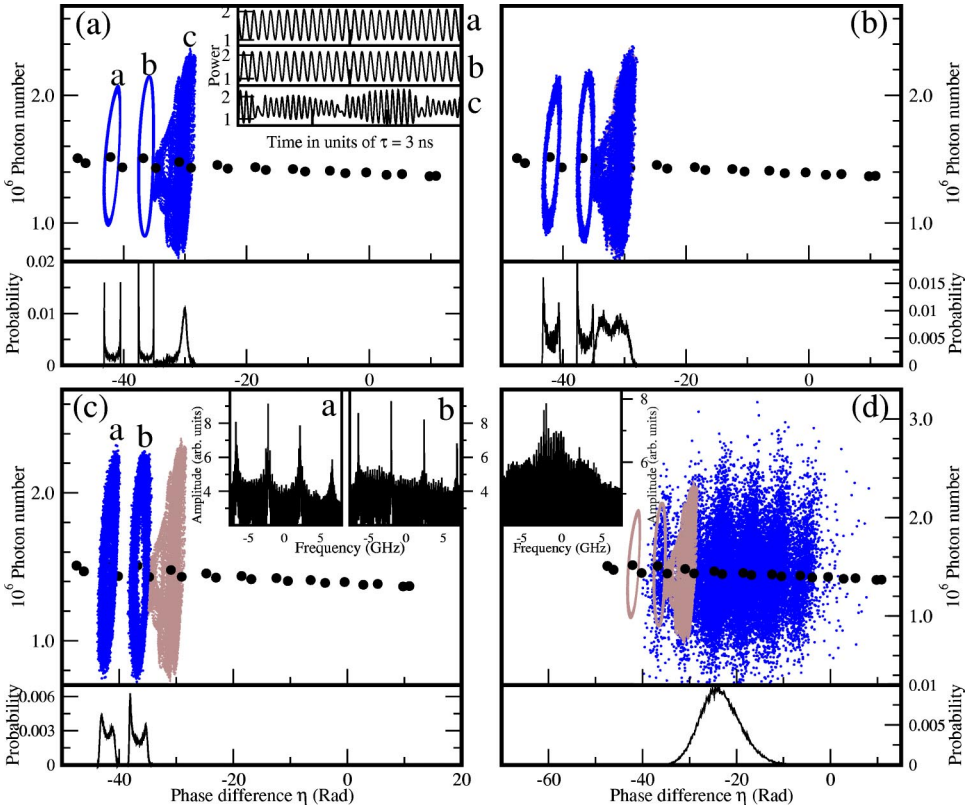

FIG. 4. (a) Phase portrait (main frame) and time series (insets) of the deterministic dynamics. The histogram of η values, as described in the text, is also shown (lower frame). $\Lambda=2$ GHz, $\omega_m=-2.6$ GHz, $\tau=3$ ns, $\gamma=6.537\times10^9$ s^{-1}, and $\alpha=5$. (b) Phase portrait and histogram of η values in the presence of spontaneous emission noise but without shot noise. Note that the dynamics resemble those in the deterministic case; even the attractors are the same. (c) Phase space portraits of the dynamics in the presence of the correct level of shot noise and spontaneous emission noise. The insets show the optical spectra. (d) Phase space portraits of the dynamics for the same case as in (c) except for the shot noise, which now is one order of magnitude larger.

to the deterministic trajectories of Fig. 4(a), but are slightly smeared due to the noise. The histograms for the variable η are also not dissimilar to the deterministic case. The conclusion one draws is that for the amount of spontaneous emission noise in this figure, the dynamics of the laser are slightly perturbed from the deterministic case, but that the deterministic attractors are still stable and this is where the system resides.

In addition to the spontaneous emission noise, if shot noise is also included ($D=1.45\times10^{16}$ s^{-1}) in the model, one sees a dramatic effect, viz., only two of the three states survive [Fig. 4(c)]. The chaotic attractor is not visited at all, *even when the simulations were started within its basin of attraction*. Clearly, the chaotic attractor is not as stable as the other two, and its basin of attraction must be rather shallow relative to those of the other attractors. A crucial variable that determines the stability of an attractor is the phase. Shot noise affects the light intensity from a semiconductor laser via the relaxation oscillations and the α parameter, which couples the intensity to the phase noise, distorts the phase of the attractor with the apparent effect of destabilizing that attractor. The deterministic fixed points are shown in Fig. 4(c), for reference, and in the plot below the phase space trajectory are the corresponding histograms of η values. From these histograms we note not only the elimination of the chaotic attractor, but also that the limit cycle is broadened.

To delve into some detail about the frequency response of a semiconductor laser under FOF, insets (a) and (b) in Fig. 4(c) contain the optical spectrum of the laser output. The center frequency of the filter is detuned from the solitary laser by -2.07 GHz, and we note from the spectra that the laser under FOF operates in a detuned mode, i.e., instead of the main peak being at 0, it is centered at -2.07 GHz. We also identify additional peaks in the spectrum of inset (a), which are offset by 0.3 GHz on either side of the main peak at -2.07 GHz. These peaks are evidence of the round trip dynamics in the laser response, corresponding to the delay time of 3 ns. We also note from inset (b) that the limit cycle consists of periodic oscillations at the center of the filter. Lastly, we also see evidence of the relaxation oscillation peaks in both spectra.

On increasing the shot noise level by one order of magnitude, to $D=1.45\times10^{17}$ s^{-1}, the resulting dynamics [displayed in Fig. 4(d)] no longer resemble that of the deterministic case. Now the system mainly resides on the ruins of an attractor that existed for larger filter detunings and is unstable at the present detuning. The optical spectrum of the attractor clearly identifies it as ''chaotic'' with the ECM frequencies still visible as a result of the light passing through the external cavity. This is consistent with the phase difference residing, for the most part, close to multiples of 2π (see histogram). This manifestation of constructive interference is not unexpected, even for high shot noise levels, since shot noise has a minimal effect on the low-frequency phase fluctuations [16,21].

Figures 4(a)–4(d) provide convincing evidence that the shot noise of the laser play a key role in determining the final form of the dynamics that are exhibited by the laser. So far we have discussed the dynamics that result for intermediate filter bandwidths ($\Lambda\sim2$ GHz). To further isolate the noise-induced alterations in laser response, and to make comparisons with optical injection, we will now concentrate on a

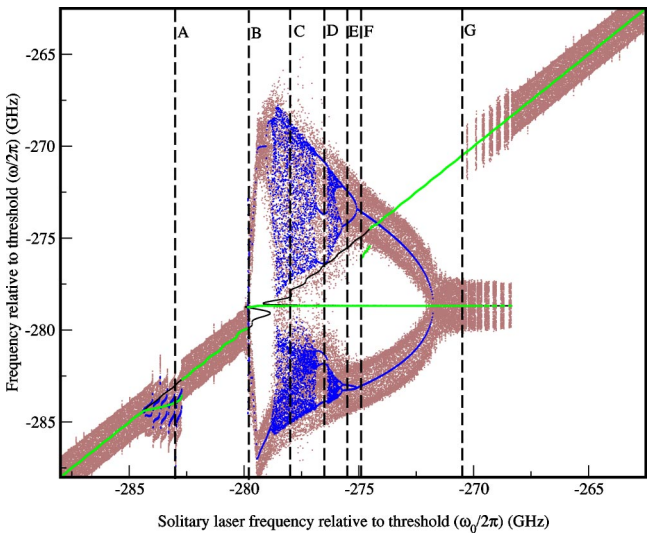

FIG. 5. Bifurcation map of FOF for the parameters in Table I. $\Lambda=66.7$ MHz, $\tau=1.5$ ns, $\gamma=13.07\times10^{9}$ s^{-1}, $\alpha=5$, and $\varepsilon=40$. The gray dots represent the intersection of the phase space trajectory with the Poincare plane in the presence of noise while the black dots show the same quantity in the absence of noise. The thin black line indicates the fixed points and the thick gray line shows the average value of the phase space trajectory over 50 external roundtrips. Phase space portraits of cases $A,B,\ldots,G$ are shown in Fig. 6.

narrow bandwidth filter, $\Lambda=66.7$ MHz, and an external cavity mode spacing of 667 MHz (i.e., delay time of 1.5 ns). The noise properties are calibrated according to Fig. 3. All other parameters were chosen to obtain a ''classical'' route in and out of chaos (Table I), i.e., a quasiperiodic route into chaos and a period doubling route out of chaos. In Fig. 5 the Poincaré intersection of the phase space trajectory is plotted in the usual (ω,ω_0) plane which displays all the possible dynamics within the laser. The filter is centered at -278.7 GHz. In this figure, the deterministic dynamics (black dots), and those in presence of noise (gray dots) are shown, along with the fixed points (black thin line) and their average values in the presence of noise (gray thick line). It is instructive to examine the details of the dynamics that are represented in Fig. 5, and so the panels in Fig. 6 show some of these in the (η,P) plane, together with the optical spectra and the RIN spectra. Figure 5 will be analyzed from left to right (decreasing pump rate), and to facilitate the discussion of Fig. 6, various parts of Fig. 5 have been labeled with letters A through G and the corresponding dynamics are shown in Figs. 6(a)–6(g), respectively.

At large positive detunings ($\omega_0<-285$ GHz), the effect of the filter on the dynamics is marginal since almost no light is transmitted back into the laser semiconductor and so only cw operation is possible. When the center of the filter is tuned to the high-frequency relaxation oscillation (RO) peak at -283 GHz (i.e., $\omega_m\approx\omega_{\mathrm{RO}}$), some of the light contained in this peak leaks back into the laser cavity. The laser perceives this as feedback and therefore starts oscillating, as depicted in Fig. 6(a). The center of these oscillations is located -1 GHz away from solitary laser operation. The origin of this 1 GHz shift can be seen by going back approximately 1 GHz in filter detuning and studying the limit cycle that arises at $\omega_0=-284$ GHz. Since the RO side peaks have a substantial width, it is possible for the laser to receive light from the high-frequency RO side peak when the filter is centered at $\omega_0=-284$ GHz. At this detuning, the amount of feedback light is very low and only a low-amplitude limit cycle can be sustained. In order for the system to maintain the limit cycle oscillations, the laser must shift its RO peak and oscillate at a higher frequency than the intrinsic relaxation oscillations at this pump level ($\omega_{\mathrm{RO}}=4.2$ GHz). In Fig. 6(a), where $\omega_m=\omega_{\mathrm{RO}}$, the laser has moved its relaxation oscillation frequency by ~1 GHz to 5.1 GHz, in order to profit maximally from the feedback. The -1 GHz detuning from the solitary laser operation is possible because the RO side peak is not infinitely narrow and therefore the laser has some ''freedom'' to adjust its frequency and attain the maximum possible output. Due to the positive value of the linewidth enhancement factor, negative detuning corresponds to higher output power. To compensate for the extra carrier depletion due to the high output, the laser goes into large-amplitude self-oscillations where the maximum of the amplitude is at 150% of the solitary laser power and the minimum is at 50% of the solitary laser power. The RIN in Fig. 6(a) confirms the higher relaxation oscillation frequency and the optical spectrum identifies the -1 GHz detuned operation. Note that the high-frequency relaxation oscillation side peak is narrower in the optical spectrum than its low-frequency counterpart because the light in the high-frequency RO peak has passed through the filter center. This locking to the high-frequency RO peak continues until $\omega_0=-282$ GHz.

It is interesting to note that the case of narrow filter FOF is in some respects similar to a semiconductor laser with optical injection, where the injection strength is a self-consistently determined quantity as described above. The dynamics of Fig. 6(a) are an example of phase unbounding of an attracting limit cycle [22] since the laser frequency locks, not to the ''injection'' frequency (i.e., the high-frequency RO peak), but ~-5.2 GHz detuned from it. This feedback mechanism via the high-frequency relaxation oscillation peak seems to occur only for sufficiently narrow filters, whereas broader filters were seen to induce feedback via the low-frequency relaxation oscillation peak [14]. For the current parameters, the low-frequency relaxation oscillation peak falls within the filter locking range, and its effects are overshadowed by the direct filter-induced dynamics in the representation of Fig. 5. Further down, we will introduce a different representation of the bifurcation map in FOF and in that representation the low-frequency RO-peak-induced dynamics are clearly visible.

As the filter center is approached, the amount of feedback light increases, inducing more complex dynamics, and in Fig. 6(b) is an example of a case on the quasiperiodic route to chaos. Here, deterministic analysis indicates operation on a torus as the only stable dynamics where the slow frequency is 66.7 MHz, i.e., the filter bandwidth. In the presence of noise the torus remains, as can be seen from the low-frequency peak in the RIN spectra. Note that the center of the attractor is at the positive-η (low-power) fixed points, whereas the ''solitary laser'' fixed point with higher intensity

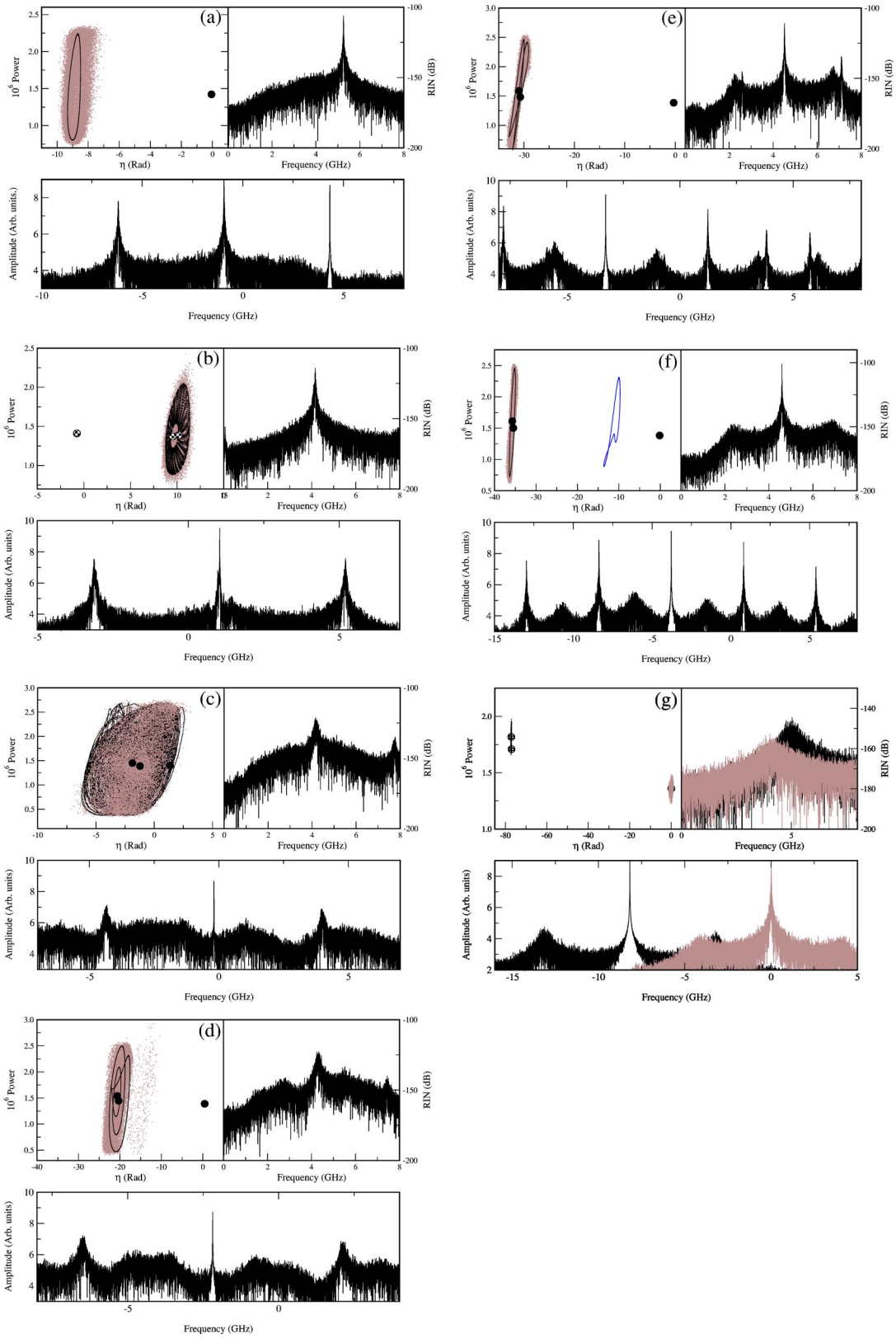

FIG. 6. Phase space portraits for the cases $A-G$ of Fig. 5. The optical spectra and the RIN spectra are also shown. Note that the scale differs in the panels. A detailed explanation for each of the cases $A-G$ is given in the text.

is not stable. Such behavior is consistent with the response of a laser subject to optical injection. The optical spectrum shows that the laser frequency locks to the injection frequency, which is 1 GHz detuned from the solitary laser frequency. Indeed, a phase-bounded torus is predicted for a laser with optical injection under similar circumstances in Ref. [22]. We note from Fig. 5 that in the deterministic case the quasiperiodic motion changes into a closed orbit on the torus after which a pocket of chaos is reached as the detuning is further decreased, whereas in the presence of noise the limit cycle abruptly changes into a chaotic attractor. In Fig. 6(c), a sample of the chaotic dynamics is shown. The ''flat'' optical spectrum, except for the wide relaxation oscillation peaks, implies that the attractor is chaotic and the central peak indicates operation on the negative-η (high-power) fixed points, consistent with the phase space portrait. The occurrence of a phase-bounded chaotic attractor is in good agreement with what has been reported for the injection laser at small negative detunings [22].

In the middle of the chaotic region of Fig. 5, a period-3 limit cycle appears, which is depicted in Fig. 6(d). Quantum noise perturbs this limit cycle and the optical spectrum in the presence of noise resembles that of a chaotic attractor rather than a period-3 limit cycle. Also, in Fig. 5, the period-3 pocket is not visible in the presence of noise (gray dots). The phase space portrait shows that, although the trajectory spends most of the time close to the deterministic period-3 limit cycle, some occasional excursions toward the solitary laser mode are made. Variations in the noise level, and even complete omission of the shot noise ($D=0$), did not change the scenario. Clearly, the period-3 limit cycle is immediately destroyed by weak noise, and instead the dynamics become chaotic with sparse isolated excursions toward the solitary laser operation.

Figure 5 shows that for the chosen parameter set, as the detuning is increased, the region of chaos is exited through a period doubling route, where the period-2 and period-1 limit cycles are shown in Figs. 6(e) and 6(f), respectively. The optical spectra identify the oscillation frequency as the relaxation oscillation frequency, which is consistent with a peak that appears at the relaxation oscillation frequency in the RIN of Fig. 6(e). Indeed, such a scenario is to be expected when a semiconductor laser is subject to optical injection [22], and predictions for such a laser say that with further detuning one obtains an inverted Hopf bifurcation that ends in a state of stable locking at negative detuning. This stable locking state is seen in Fig. 6(g) as the very narrow peak in the optical spectrum at the center of the filter at ~ -8 GHz. In the absence of noise the period-1 limit cycle that occurs at point F in Fig. 5 [see Fig. 6(f)], coexists with another limit cycle, which ''floats'' between the solitary laser and the filter center. However, noise destabilizes this attractor.

At large negative detunings (point G in Fig. 5) the amount of feedback light passing through the filter is very low and is insufficient to induce dynamics. However, cw locking to the filter center becomes possible and a global cw bistability between the filter center and the solitary laser appears. The superimposed optical spectra in Fig. 6(g) show two distinguishable states of operation, separated by $\omega_m/2\pi \sim 8$ GHz,

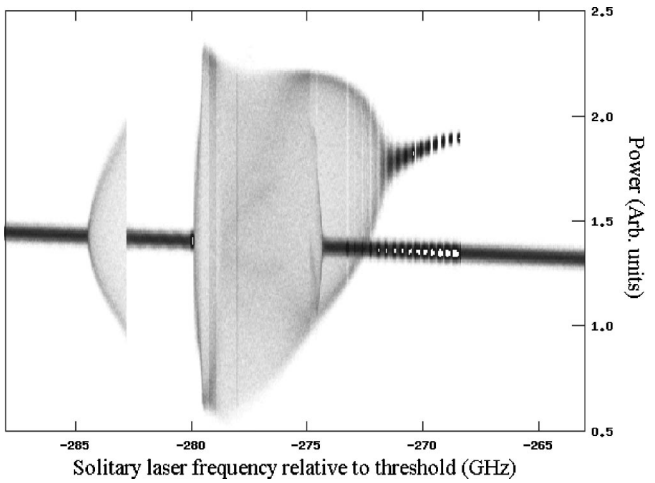

FIG. 7. Probability density of operation on a certain power level versus the solitary laser frequency for the same case as Fig. 5. Dark regions represent high probability while lighter regions represent low probability. Note the discontinuous locking behavior at the beginning of the filter locking region ($\omega_0 \in [-273,-269$ GHz]), and the coexistence of the two attractors between -275 and -269 GHz.

which correspond to the solitary laser frequency and the filter frequency. The linewidth at solitary laser operation is ~ 20 MHz while operation at the center of the filter corresponds to ~ 1 MHz linewidth. During operation at the center of the filter, the light passes through the filter center and because of the narrow filter width is ''cleaned.'' Hence, operation at the center of the filter has a smaller linewidth. This is an example of an ''injection-locked'' state. The apparent coexistence with the state of nearly solitary laser operation is a manifestation of the self-consistent setting of the injection rate; namely, the system can operate either at solitary laser frequency and thus be subject to very little injection, or at the filter frequency and so fully profit from the feedback, i.e., be subject to large injection strengths.

In Fig. 7 we show a different bifurcation map of FOF, i.e., the power probability density versus the solitary laser frequency, where the power signal has been low-pass filtered to mimic a 1 GHz bandwidth photodetector. Here, the solitary-laser-centered operation corresponds to the nearly horizontal line, whereas the filtered-centered operation corresponds to the upper branch. The dark regions identify high probability while lighter regions correspond to low probability. In the representation used in Fig. 5, the solitary laser fixed point seems to destabilize once the operation at the filter center becomes possible ($\omega_0 \in [-275,-270]$ GHz). On the contrary, Fig. 7 shows a bistable scenario in the same frequency range, where a cw state at solitary laser operation coexists with the limit cycle at the filter center. This cw state bifurcates to a limit cycle as the filter center is approached further ($\omega_0 \sim -275$ GHz). This limit cycle is the low-frequency counterpart of the limit cycle A [Fig. 6(a)]. In Ref. [12], Guidici *et al.* report on transition from cw-solitary laser operation to limit cycle operation at the filter center when the feedback strength is increased. Such a scenario can be seen in Fig. 5 when starting at -265 GHz one tunes the laser down in frequency and then encounters the period-doub-

ling route into chaos. The two branches in Fig. 7 at $\omega_0 \in [-275,-270]$ GHz indicate the possibility of hysteresis, which was indeed also observed in Ref. [12]. Also seen in Fig. 7 is a discontinuous trace at the filter center around -270 GHz, which indicates that this fixed point is not stable throughout the whole locking range. This is a manifestation of the phase contribution from the filter, which is described by the arctangent term in Eq. (10). Detuning variations will cause a change in the interference conditions between the external and internal light and therefore change the stability of the fixed point. Figure 7 is in a form that can be compared directly to a measurement of the output power with a 1 GHz photodiode.

V. SUMMARY AND CONCLUSIONS

We theoretically analyzed the dynamics of a semiconductor laser with filtered optical feedback in the presence of noise, and by comparing with the deterministic analysis elucidated the effects on quantum noise on laser response. Although shot noise is traditionally neglected in studying semiconductor lasers, our analysis included shot noise. The results indicated that, consistent with the predictions of Henry *et al.* [21], shot noise had practically no effect on the fixed points of the laser, i.e., on the steady-state characteristics. On the other hand, if the semiconductor laser exhibits dynamics, we find that shot noise has a substantial influence and cannot be neglected. Since shot noise level is an intrinsic property of the semiconductor laser, we conclude that the dynamics of a semiconductor laser with filtered optical feedback will strongly depend on the shot noise property of the specific laser design and on the bandwidth of the external filter.

Noise automatically perturbs the phase space trajectory and a large region of phase space can thus be ''probed'' to acquire information on the stability of attractors. In the results reported in Fig. 4 we demonstrated the sensitivity of the dynamics, and of specific attractors, to shot noise levels. Specifically, variations in the magnitude of shot noise level can alter the stability and existence of specific attractors.

In Ref. [14], the deterministic dynamics were investigated for moderately narrow filter bandwidths ($\sim$1 GHz). When the bandwidth of the filter is smaller than the external cavity mode spacing, the scenario is expected to resemble that of optical injection with few fixed points and low-dimensional dynamics. Our results do indeed confirm this expectation. We concentrated on the narrow bandwidth regime to identify the noise-induced changes in the dynamics for a very simple sequence of bifurcations and also to emphasize the injection character of narrow-bandwidth-filtered feedback. Two classical routes into and out of chaos were investigated and the period-doubling route was found in the presence of noise while the quasiperiodic route is no longer present. In [12] Giudici *et al.* measured filtered-feedback dynamics using the feedback rate as the bifurcation parameter. They showed periodic oscillation at the filter center, as shown in Fig. 6(f), and cw operation at solitary laser frequency (~ -269 GHz in Fig. 7), and switching between the two could be achieved by means of varying the feedback rate. Hysteresis was also shown, indicating bistable behavior. In our analysis the feedback rate is fixed and the detuning is used as the bifurcation parameter. In Figs. 6(f) and 6(g), the two states of interest are shown and Fig. 7 clearly depicts the bistability in this region.

For narrow bandwidth filters, the dynamics do not change significantly when the shot noise level is increased, implying that the feedback light is ''cleaned'' in the external cavity and the dynamics are mainly filter induced. It has been shown by Yabre *et al.* [26] that in case of injection the slave laser will copy the noise properties of the injected signal. In many of the cases depicted in Fig. 6 the optical spectrum shows the feedback signal as a detuned, narrow peak at the filter center. The robustness of the dynamics as the noise level is changed indicates that the feedback light is deciding the nature of the dynamics, unlike for broad filters (Fig. 4) where the shot noise level is very influential in determining the nature of the dynamics. We therefore conclude, in agreement with [9,10], that narrow bandwidth filters will stabilize the FOF-system even in the presence of noise and that for these bandwidths the dynamics resemble in several aspects that of a semiconductor laser with optical injection [22].

Finally a histogram of operation versus bifurcation parameter was presented (Fig. 7). This plot can directly be compared with experimental data, since it shows the output power of the laser detected by a 1 GHz bandwidth photodiode. The bifurcations up to period 2 can clearly be identified, and the complementary information on operation and bifurcation of the solitary laser frequency can also be extracted from this plot, since it shows the statistics of the full phase space trajectory and not merely an intersection with a plane.

ACKNOWLEDGMENTS

G.V. is pleased to acknowledge the hospitality of the Vrije Universiteit, Amsterdam and financial support from NSF.

[1] See, e.g., *Nonlinear Laser Dynamics: Concepts, Mathematics, Physics, and Applications International Spring School*, edited by B. Krauskopf and D. Lenstra, AIP Conf. Proc. No. 548 (AIP, Melville, NY, 2000).
[2] Quantum Semiclassic. Opt. **9**, (1997), special issue on fundamental nonlinear dynamics of semiconductor lasers.
[3] G. H. M. Van Tartwijk and D. Lenstra, Quantum Semiclassic. Opt. **7**, 87 (1995).
[4] A. Murakami and J. Ohtsubo, IEEE J. Quantum Electron. **34**, 1979 (1998).
[5] B. Krauskopf, G. R. Gray, and D. Lenstra, Phys. Rev. E **58**, 7190 (1998).
[6] B. Tromborg, J. H. Osmundsen, and H. Olsen, IEEE J. Quantum Electron. **20**, 1023 (1984).
[7] R. Lang and K. Kobayashi, IEEE J. Quantum Electron. **16**, 347 (1980).
[8] D. Lenstra, B. H. Verbeek, and A. J. Den Boef, IEEE J. Quantum Electron. **21**, 674 (1985).

[9] H. Li and N. B. Abraham, IEEE J. Quantum Electron. **25**, 1782 (1989).
[10] C. Etrich, A. W. McCord, and P. Mandel, IEEE J. Quantum Electron. **27**, 937 (1991). See also H. Yasaka and H. Kawaguchi, Appl. Phys. Lett. **53**, 1360 (1998).
[11] M. Yousefi and D. Lenstra, IEEE J. Quantum Electron. **35**, 970 (1999).
[12] M. Giudici, L. Giuggioli, C. Green, and J. R. Tredicce, Chaos, Solitons Fractals **10**, 811 (1999).
[13] A. P. A. Fischer, O. K. Andersen, M. Yousefi, and D. Lenstra, IEEE J. Quantum Electron. **36**, 375 (2000).
[14] M. Yousefi, D. Lenstra, G. Vemuri, and A. P. A. Fischer, IEE Proc.: Optoelectron. **148**, 233 (2001).
[15] T. Heil, I. Fischer, and W. Elsaesser, Phys. Rev. A **60**, 634 (1999).
[16] K. Petermann, *Laser Semiconductor Modulation and Noise* (Kluwer, Dordrecht, 1988); see also J. Wang and K. Petermann, IEEE J. Quantum Electron. **27**, 3 (1991).
[17] A. Gavrielides, T. C. Newell, V. Kovanis, R. G. Harrison, N. Swanston, Yu Dejin, and Lu Weiping, Phys. Rev. A **60**, 1577 (1999).
[18] R. Roy and K. S. Thornburg, Jr., Phys. Rev. Lett. **72**, 2009 (1994).
[19] L. Larger, J. P. Goedgebuer, and F. Delorme, Phys. Rev. E **57**, 6618 (1998).
[20] S. Sivaprakasam and K. A. Shore, IEEE J. Quantum Electron. **36**, 35 (2000).
[21] C. H. Henry, IEEE J. Quantum Electron. **18**, 259 (1982); see also **19**, 1391 (1983).
[22] S. Wieczorek, B. Krauskopf, and D. Lenstra, Opt. Commun. **172**, 279 (1999).
[23] W. H. Press, S. A. Teukolsky, W. T. Vetterling, and B. P. Flannery, *Numerical Recipes in C*, 2nd ed. (Cambridge University Press, New York, 1994).
[24] D. Kahaner, C. Moler, and S. Nash, *Numerical Methods and Software* (Prentice-Hall, Englewood Cliffs, NJ, 1989), Chap. 10.
[25] E. Ott, *Chaos in Dynamical Systems* (Cambridge University Press, Cambridge, 1993).
[26] G. Yabre, H. de Waardt, P. A. v. d. Boom, and G.-D. Khoe, IEEE J. Quantum Electron. **36**, 385 (2000).